Enhanced Photocatalytic Activity of Vertically-Aligned Transition Metal-Doped Zinc Oxide Nanorods Synthesized by a Facile Electrochemical Method

Shaochun Yuan[1], Min Wang[1,*], Bo Lv[2,*]

[1] Chongqing Engineering Laboratory of Environmental Hydraulic Engineering, Chongqing Jiaotong University, Chongqing, 400074, PR China
[2] Engineering Research Center for Sponge City Construction of Chongqing, Chongqing, 400020, PR China
[*]E-mail: wangm@cqjtu.edu.cn (Min Wang) and haimiancq@163.com (Bo Lv)

The present work aims to study the photocatalytic activity of vertically-aligned $Mn_xZn_{1-x}O$ nanorods (x = 0, 0.05, 0.1, 0.15 and 0.2) by optical, electrochemical analyses and rhodamine B (RhB) degradation. Therefore, high density of $Mn_xZn_{1-x}O$ nanorods array were electrodeposited on ITO coated glass and GCE substrates. The XRD analysis indicated the wurtzite structure for ZnO and confirmed formation of Mn_2O_3 impurity phase in $Mn_xZn_{1-x}O$ samples. Optical study showed the edges of absorption spectra were blue-shifted with increasing Mn concentrations. The photocatalytic performance of $Mn_xZn_{1-x}O$/GCE was studied through electrochemical determination of Gallic acid and RhB degradation. Amperometric analysis exhibited that the electrocatalytic current density was increased with increasing the dopant concentration in ZnO nanorods. The photoelectrocatalytic capability was studied in dark and under light irradiation conditions. Results showed that the stability, detection limit, sensitivity and photocatalytic activity of $Mn_xZn_{1-x}O$/GCE were improved remarkably by doping Mn in ZnO lattice. Furthermore, $Mn_xZn_{1-x}O$ nanorods array displayed a desirable performance on RhB photocatalytic degradation.

1. INTRODUCTION

The photocatalytic reactions and photocatalytic degradation are mainly attributed to semiconductors which possess the ability to absorb light and generate the charge carriers [1, 2]. This mechanism takes place through absorption of photon energy equal to or more than the optical band gap energy of semiconductors and the absorbed photon results in the creation of electron-hole pair [3].

When an electron-hole pair migrates to the semiconductor surface, it can interact with the surface adsorbed reactants to simplify the redox process. Photocatalysis is considered as a promising technique to develop the remediation of wastewater and green energies such as solar cells [4, 5].

Titanium dioxide (TiO_2) is one of the most studied semiconductors with a broad spectrum of activity forms. It is considered as the most efficient photocatalyst to water treatment and transform toxic and non-biodegradable organics into CO_2, H_2O and inorganics [6-10]. However, its photocatalytic application is limited because of its wide band gap (3.2 eV) and high rate of electron-hole recombination because of absent or loss of energy in semiconductor [11, 12]. Therefore, improvement in the efficiency of photocatalytic properties of semiconductors and typically TiO_2 and reduction electron-hole recombination rate is needed. Accordingly, band gap engineering and development the light absorption range are carried out by application dopants, composites and multilayer thin films. Surface properties and high-crystallinity of photocatalyst are some important factors in electrons and holes transportation to the catalyst surface. These factors can reduce the recombination centers of electrons and holes through decreasing the defect density and grain boundaries [13-15]. Therefore, nanotechnology is a great approach to promote the photocatalytic properties by modification of the surface properties, increasing the effective surface area, facilitating the carrier transport and enhancing the photocatalytic degradation performance.

Zinc oxide (ZnO) as nontoxic, low cost, environmentally friendly semiconductor, with wide band gap (3.37 eV) is used in many fields such as optoelectronic, solar cell, laser diodes, light emitting diodes, UV-light emitters, anti-UV additives, ceramics, sensors, super-capacitors, piezoelectric transducers, sensors and photocatalysts [16-18]. Moreover, its optical band gap energy is close to that of TiO_2 which makes it a suitable candidate for use in photocatalytic application. Furthermore, many studies were carried out to band gap engineering and development the ZnO based photocatalysts. For example, Nagaraju et al. [19] reported good photocatalytic performance of ZnO nanoparticles to degradation of methylene blue dye under both UV and Sunlight irradiation. Tian et al. [20] showed the ZnO nanoparticles have excellent photocatalytic reaction towards photodegradation of organic pollutants (superior to Degussa P25 TiO_2). It is important to note that photocatalytic activities are generally controlled by band gap energy and hydroxyl radicals [21, 22]. The low-charge separation efficiency is the main limitation of application of ZnO photocatalysts. Thus, doping process with non-metallic materials (C, S, N) and metallic materials (Mo, Cu, Co, Fe, Ag, Y, Hf, Mg, Sn, Ni, Bi, Al, Ce, Nd, Eu, Sm, La, Gd) was applied to narrow the band gap energy to the ultraviolet-visible region or upwardly shift the valence band energy [23, 24]. Manganese (Mn) is a cheap and frequent metal that is selected as a transition metal dopant of ZnO in this study. Mn was studied for fabrication the batteries and gas sensors [25-27]. Therefore, in this study the photocatalytic performance of $Mn_xZn_{1-x}O$ nanorods/GCE were investigated by optical and electrochemical analyses.

2. MATERIALS AND METHODS

The transition metal doped ZnO nanorods in $Mn_xZn_{1-x}O$ (x = 0, 0.05, 0.1, 0.15 and 0.2 are Mn concentration as transition metal dopant refer 5%, 10%, 15% and 20%, respectively) formula were

synthesized using electrodeposition method [28]. The mixture of 0.1 M of zinc chloride (> 99%, Merck, Germany) and desired concentration of manganese chloride (98%, Merck, Germany) were prepared with deionized water. The solution preparation steps were carried out under thermal treatment in magnetic-stirrer devices. The prepared solution was transferred to electrochemical cell which containing clean glassy carbon electrode (GCE) and indium tin oxide (ITO) coated glass as working electrodes for electrochemical and optical studies, respectively, platinum wire as counter electrode and Ag/AgCl/(sat KCl) as reference electrode. The electrodeposition process was carried out in stirring solution condition under current densities of 4 mA/cm^2.

The structure of synthesized $Mn_xZn_{1-x}O$ nanorods was analyzed by scanning electron microscopes (SEM; S-4300, *Hitachi*, Japan). Xpert Pro X-ray diffractometer (XRD) with 1.5404 Å (Cu Kα) in wavelength and 40KV/30 mA in power was applied to study the crystal structure of $Mn_xZn_{1-x}O$ nanorods.

Photoelectrochemical studies were performed in the electrochemical cell with 0.1 M phosphate buffer solutions (PBS) which provided from H_3PO_4 (85%, Fondland Chemicals Co., Ltd., China) and NaH_2PO_4 (>99%, Merck, Germany). The pH of PBS was adjusted with HCl and NaOH solutions were applied to adjustment of the phosphate buffer solutions pH. Auto lab modular electrochemical system (*Autolab PGSTAT302N* Metrohm Herisau, Switzerland) was used for electrochemical studies. Photocatalysis experiments were conducted on a photoreaction apparatus (125 W high-pressure mercury lamp) with a 420 nm cut-off filter served as a UV light source. The concentration of the RhB aqueous solution is 45 mg/L. Using the degradation rate and k (degradation rate constant) as the index to evaluate the catalytic degradation ability of the prepared products.

3. RESULT AND DISCUSSION

Figure 1 shows top view SEM images of the electrodeposited doped and undoped ZnO nanorods arrays on GCE substrate. As seen, a hexagon-shaped, uniform and dense array of vertically-aligned ZnO nanorods was fabricated on GCE substrate. The average diameter and length of Mn-doped ZnO nanorods are about 250 nm and 2 μm, respectively.
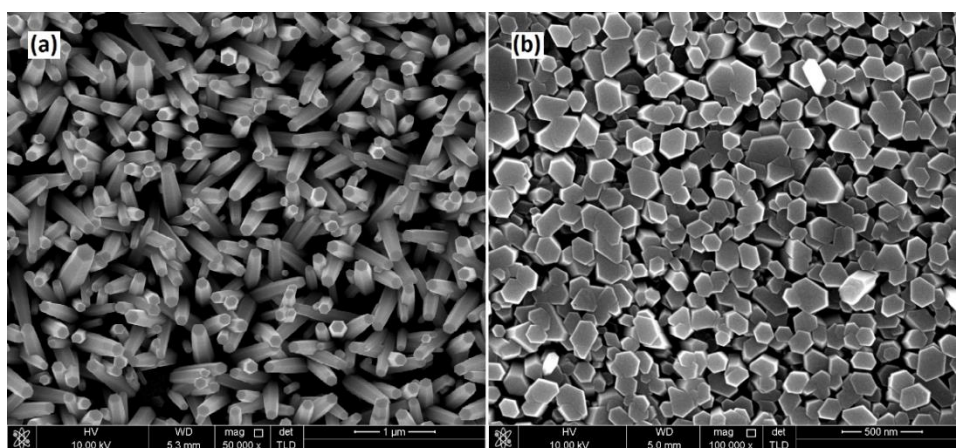

Figure 1. SEM images of (a) undoped ZnO nanorods (b) $Mn_xZn_{1-x}O$ nanorods on GCE

XRD patterns of $Mn_xZn_{1-x}O$ show the peaks at 31.78°, 34.43°, 36.31°, 47.54°, 56.60°, 62.90°, 66.41°, 67.93°, 69.10°, and 77.01° which exhibiting the formation of wurtzite structure for ZnO with (100), (002), (101), (102), (110), (103), (200), (112), (201), and (202) planes, respectively [29, 30].
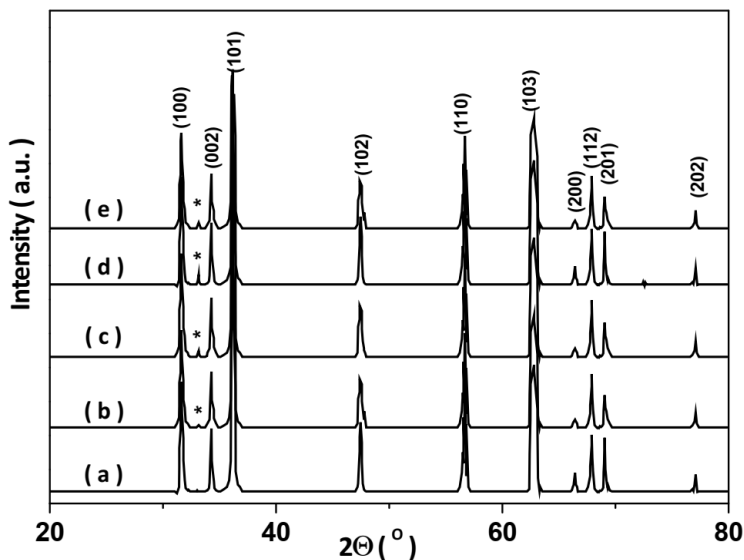

Figure 2. XRD patterns of (a) ZnO, (b) $Mn_{0.05}Zn_{0.95}O$, (c) $Mn_{0.10}Zn_{0.90}O$, (d) $Mn_{0.15}Zn_{0.85}O$ and (e) $Mn_{0.20}Zn_{0.80}O$

As shown in Figure 2, the Mn_2O_3 impurity phase peak at 33.00° (denoted with symbol *) corresponding to (222) orientation was observed for doped samples according to standard JCPDS data reference (No. 00-024-0508). It should be considered that the solubility of Mn in a ZnO structure is below 2 % [31-33].

The recorded UV-Vis absorption spectra of $Mn_xZn_{1-x}O$ nanorods are reported in Figure 3. As seen, the similar types of absorption spectra were recorded for all samples. The Maximum of adsorption was taken in the UV region (>350 nm). Moreover, the positions of the Maximum absorption spectra are blue-shifted with increasing dopant concentrations which are attributed to the variation in the optical band gap value. The obtained values of the absorption wavelengths for ZnO, $Mn_{0.05}Zn_{0.95}O$, $Mn_{0.10}Zn_{0.90}O$, $Mn_{0.15}Zn_{0.85}O$ and $Mn_{0.20}Zn_{0.80}O$ nanorods are 345, 334, 337, 335 and 331 nm, respectively. It can be suggested that the blue-shift is correlated to doping of Mn in ZnO nanorods through replacement of Zn in the ZnO lattice by Mn. The increasing Mn concentration in nanorods structure leads to increased charge carrier concentration [34]. Moreover, introducing the Mn^{3+} and Mn^{4+} ions with higher positive charges increases the zinc interstitials and oxygen vacancy concentrations which donates free charge carriers. In addition, this illustrates that the band gap of the ZnO nanorods increases with the doping concentration of the Mn^{2+} ion. The increase in the band gap or blue-shift can be explained by the Burstein-Moss effect [35]. In This phenomenon, the Fermi level merges into the conduction band with increasing of the carrier concentration. Therefore, the low energy transitions are blocked. The results are in good agreement with the results presented by Sabri and Menon [36, 37].
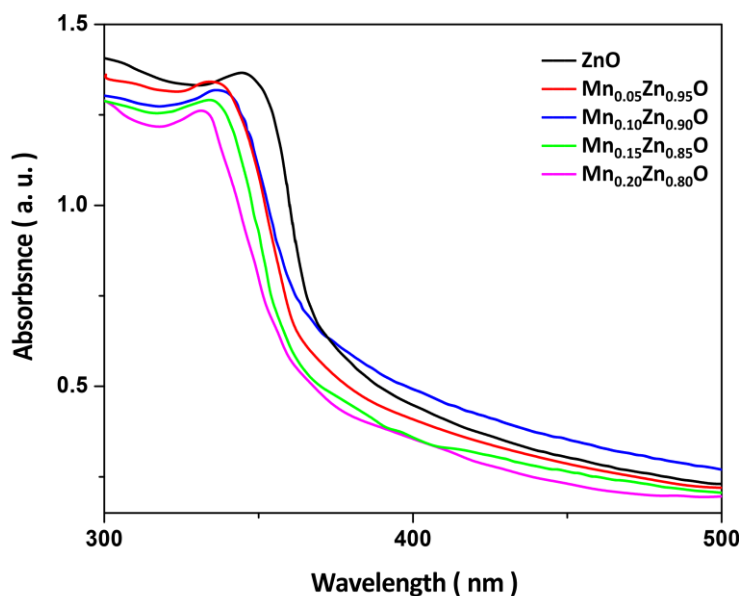
Figure 3. The recorded UV-Vis absorption spectra of $Mn_xZn_{1-x}O$ nanorods

In order to study electrochemical properties of GCE and ZnO nanorods/GCE and $Mn_{0.05}Zn_{0.95}O$ nanorods/GCE, the cycle voltammetry responses of prepared electrodes in 0.1 M PBS pH 4.0 at a scan rate of 100 mV s^{-1} in the potential range of -0.05 to +0.65 V were recorded before and after injection of 10 µM Gallic acid (Figure 4).
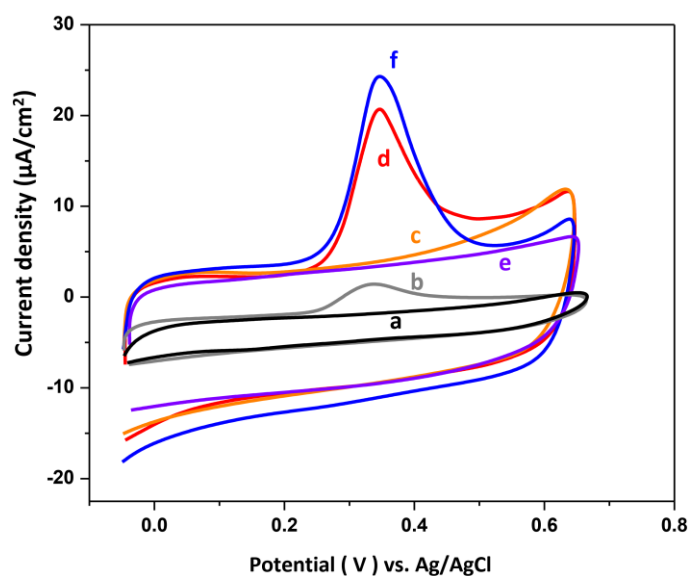

Figure 4. The cycle voltammetry responses in 0.1 M PBS pH 4.0 at a scan rate of 10 mV s^{-1} of (a) GCE, (c) ZnO nanorods/GCE and (e) $Mn_{0.05}Zn_{0.95}O$ nanorods/GCE in absent of 10 µM Gallic acid and (b) GCE, (d) ZnO nanorods/GCE and (f) $Mn_{0.05}Zn_{0.95}O$ nanorods/GCE, in present of 10 µM Gallic acid.

Figure 4d shows that oxidation peak current improved by modification of the GCE surface with doped and undoped ZnO nanorods. The high aspect ratio and high porosity of nanorods structure cause an increase in the active site and effective surface area and finally electrocatalytic current density of modified electrodes [38, 39]. As seen in Figure 4f, ZnO and $Mn_{0.05}Zn_{0.95}O$ nanorods on GCE lead to negative shift of potential peak because nanorods change in electron transfer rate between the solution and electrode surface due nanostructures and higher conductivity of metallic dopant [40]. In addition, $Mn_{0.05}Zn_{0.95}O$ nanorods /GCE shows the more sensitivity to determination of Gallic acid.
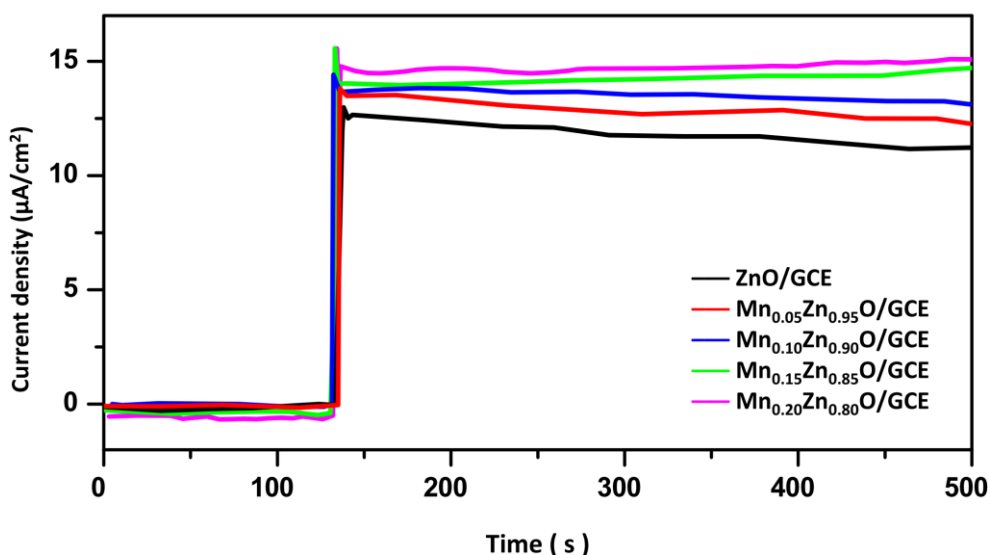

Figure 5. The recorded amperometric responses of $Mn_xZn_{1-x}O$/GCE in 0.1 M PBS pH 4.0 at 0.35 V with one injection of 10 µM Gallic acid solution

Table 1. Results of the electrocatalytic current density responses of $Mn_xZn_{1-x}O$/GCE to injection Gallic acid.

Sample	x	Electrocatalytic current density ($\mu A/cm^2$)
ZnO /GCE	0	12.14
$Mn_{0.05}Zn_{0.95}O$ /GCE	0.05	13.07
$Mn_{0.10}Zn_{0.90}O$ /GCE	0.1	13.66
$Mn_{0.15}Zn_{0.85}O$ /GCE	0.15	14.30
$Mn_{0.20}Zn_{0.80}O$ /GCE	0.20	14.69

Therefore, for determination the dopant concentration effect on electrocatalytic properties of modified electrode, the amperometric responses of $Mn_xZn_{1-x}O$/GCE (x = 0, 0.05, 0.1, 0.15 and 0.2) were recorded in 0.1 M PBS pH 4.0 in the potential of 0.35V with injection of 10 µM Gallic acid. Figure 5 displays electrocatalytic current density and stability response of $Mn_xZn_{1-x}O$/GCE to injection Gallic acid. The details of the amperometric responses are presented in Table 1. There are observed no high electrocatalytic effects with increasing the dopant concentration in ZnO nanorods. The fast and high electrocatalytic current density responses are belonging to $Mn_{0.15}Zn_{0.85}O$ nanorods/GCE and

$Mn_{0.20}Zn_{0.80}O$ nanorods/GCE of 14.69 $\mu A/cm^2$ and 14.30 $\mu A/cm^2$, respectively. Studying the stability of electrodes responses indicates the $Mn_{0.15}Zn_{0.85}O$ nanorods/GCE possess lowest change in electrocatalytic current density (2%) after 6 minutes of injection Gallic acid. Therefore, $Mn_{0.15}Zn_{0.85}O$ nanorods/GCE was chosen for further electrochemical studies.

Table 2. Effects of various interfering species on the determination of Gallic acid by $Mn_{0.15}Zn_{0.85}O$ nanorods/GCE

Specie	Added (mM)	Electrocatalytic current density ($\mu A/cm^2$)	RSD (%)	Specie	Added (mM)	Electrocatalytic current density ($\mu A/cm^2$)	RSD (%)
Gallic acid	0.1	123.91	±0.97	ascorbic acid	1	0.8	±0.9
Ca^{2+}	1	0.55	±0.01	benzoic acid	1	1.0	±0.05
Cl^-	1	0.41	±0.02	citric acid	1	0.88	±0.02
CO_3^{2-}	1	0.99	±0.05	glucose	1	0.71	±0.03
Cu^{2+}	1	0.78	±0.02	phenol	1	0.66	±0.02
Fe^{3+}	1	0.77	±0.01	Quercetin	1	1.02	±0.01
K^+	1	0.96	±0.04	salicylic acid	1	1.05	±0.03
Na^+	1	0.52	±0.05	sorbic acid	1	0.95	±0.05
NO^{3-}	1	0.48	±0.03	tartaric acid	1	0.90	±0.04
PO_4^{3-}	1	0.80	±0.03	uric acid	1	0.81	±0.07

Table 3. Results of determination of Gallic acid in green tea and drink tea samples (n = 5)

Samples	Added (µM)	Fund (µM)	Recovery (%)	RSD (%)
green tea	5	4.85	97.1	1.2
	10	9.78	97.8	1.5
	15	14.65	97.6	0.9
	20	19.25	96.2	2.1
	30	31.02	103.4	1.8
drink tea	5	4.73	94.6	1.9
	10	9.65	96.5	2.5
	15	14.33	95.5	1.8
	20	19.48	97.4	2.5
	30	30.05	100.1	3.1

Selectivity and interference response of $Mn_{0.15}Zn_{0.85}O$ nanorods/GCE was studied to determine the gallic acid using amperometry technique. Study was performed in the presence of different analytes. Table 2 depicts the results of a recorded amperometrogram of $Mn_{0.15}Zn_{0.85}O$ nanorods/GCE in 0.1 M PBS pH 7.0. at 0.35V in additions of 0.1 mM Gallic acid solution followed by successive additions of 1 mM of various substances. The results illustrate that the modified electrode showed a

clear and selective response to all additions of Gallic acid solution. The modified electrode did not show any significant response for the additions of other analytes. In addition, the presented analytes in Table 2 do not interfere with determination of Gallic acid on $Mn_{0.15}Zn_{0.85}O$ nanorods/GCE surface.

　　　To study the applicability of the prepared electrode in real samples, the concentration of Gallic acid in diluted drink tea and green tea (with PBS) samples was evaluated by amperometry technique and applying the standard addition method and recovery studies in 0.1 M PBS of pH 7.0 at 0.35V. The results of this study are illustrated in Table 3. As shown, quantitative recoveries are found in the acceptable range for both samples and the RSD values of samples are less than 3.1%. Therefore, these observations confirm the practical application of $Mn_{0.15}Zn_{0.85}O$ nanorods/GCE as a reliable sensor for the detection of Gallic acid in real samples.
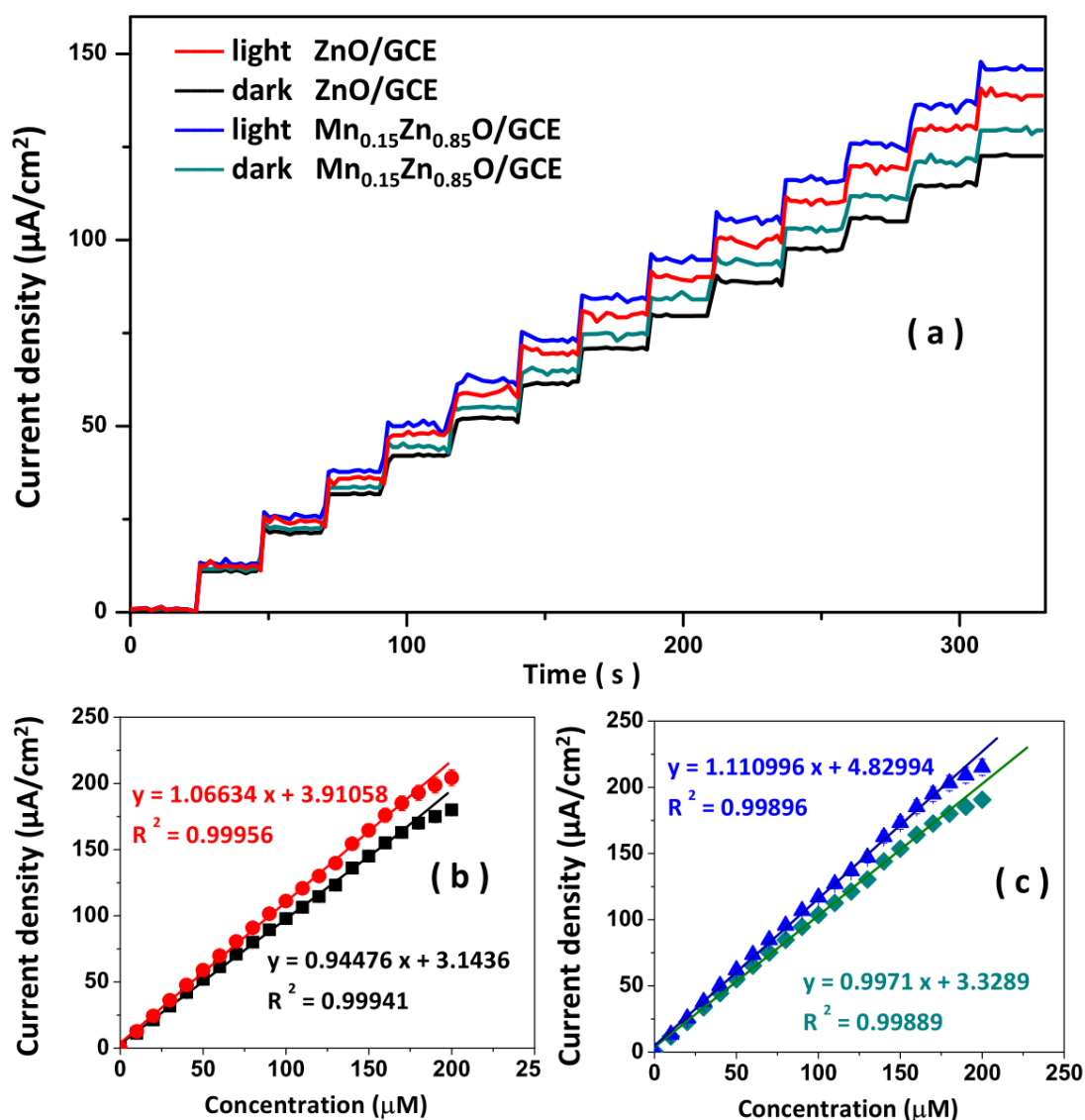

Figure 6. (a) The recorded amperometric response of ZnO nanorods/GCE and $Mn_{0.15}Zn_{0.85}O$ nanorods/GCE in 0.1 M PBS pH 4.0 at 0.35 V in successive injections of 10 µM Gallic acid solution; the plots of calibration graphs of (b) ZnO nanorods/GCE and (c) $Mn_{0.15}Zn_{0.85}O$ nanorods/GCE which investigated in dark and under light irradiation conditions.

The photoelectrocatalytic ability of the modified glassy carbon electrode was investigated in dark and under light irradiation conditions, and the results were shown in Figure 6.

Figure 6a shows the amperometric responses of the ZnO nanorods/GCE and $Mn_{0.15}Zn_{0.85}O$ nanorods/GCE in 0.1M PBS pH 4.0 at 0.35 V in successive injections of 10 µM Gallic acid solution in darkness and under visible light. As observed, the catalytic current responses were increased remarkably under illumination condition for both modified electrodes. Figure 6b and c display the linear calibration graphs of both electrodes that obtained sensitivities, detection limit and linear range of modified electrodes in both conditions were reported in Table 4. Therefore, the presence of doped and undoped ZnO nanorods leads to increased electrocatalytic activity because of generation of photo-excited electron–hole pairs in the ZnO nanorods under light irradiation. It can be considered the oxidation of Gallic acid was catalyzed by electrons of ZnO conducting bound. Therefore, photo-illumination can promote the rate of electron transfer in the electrochemical process. Moreover, study of Mn doping effect on photocatalytic activity of ZnO nanorods shows more catalytic current than undoped sample under illumination condition because of increasing the electrical conductivity through introduction of metal in semiconductor network of ZnO and increasing the free carrier concentration which donated by zinc interstitials and oxygen vacancy defects. Moreover, doping with Mn leads to formation of electron traps which decrease the pair recombination rate [41, 42]. It has been found that doping is an effective process in the photocatalytic activities only when added in optimum concentrations [41].
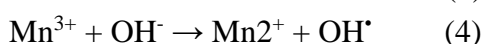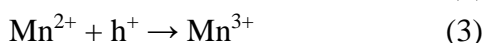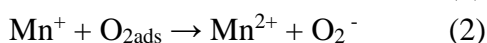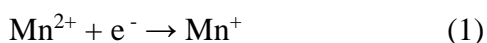
Table 4. Analytical parameters of determination Gallic acid by ZnO/GCE and $Mn_{0.15}Zn_{0.85}O$ nanorods/GCE

Electrodes	Technique	Light	detection limit (µM)	Linear range (µM)	Sensitivity (µA / cm². µM)
ZnO /GCE	Amperometry	on	0.028	10–180	1.06634
		off	0.031	10-180	0.94229
$Mn_{0.15}Zn_{0.85}O$ /GCE	Amperometry	on	0.027	10-190	1.1109
		off	0.030	10-190	0.9971

For examination the repeatability and reproducibility of modified electrodes, the amperometric responses were recorded under darkness and successive periodic turn on and off (visible and UV) light conditions for $Mn_{0.15}Zn_{0.85}O$ nanorods/GCE electrodes in 0.1M PBS pH 4.0 at 0.35 V in injections of 100 µM Gallic acid (Figure 7).

As seen, after turning off the light source the current response immediately returned to its original value while the light was turned on, instantly catalytic current was increased. The value of current in darkness and light irradiation were recorded in constant values which indicate the reversible and stable photo-induced catalytic activity of modified electrodes. By considering the variation in the absorbance spectra of doped ZnO samples in the UV region, the response of electrodes under irradiation the UV light was also examined. The result showed more photocatalytic current than visible light irradiation condition. Investigations on doped and undoped ZnO showed that the band gap value

of these samples was about 3.2 - 3.4 eV [43]. When the photons are irradiated on these samples which the energy of the photon corresponds to the energy of band gap, the required energy for generation the pair electron-hole is provided and the irradiated photon is absorbed, as consequence the excited electron is transferred from valence to conduction band. The enhancement in visible-light photocatalytic activity of Mn doped ZnO with multivalent forms (Mn^{2+}/Mn^{3+}) can be explained as follows: Mn ions substitute for Zn^{2+} ions in the ZnO wurtzite lattice leads to generation an electronic configuration change because of the ionic radius diversity. To restitute its stable electronic configuration, more oxygen (O_{2ads}) and hydroxide ions (OH^-) would be adsorbed onto the surface to formation superoxide radicals (O_2^-) and hydroxyl radicals ($OH^\bullet$) through the following reactions [44]:

$$Mn^{2+} + e^- \rightarrow Mn^+ \qquad (1)$$
$$Mn^+ + O_{2ads} \rightarrow Mn^{2+} + O_2^- \qquad (2)$$
$$Mn^{2+} + h^+ \rightarrow Mn^{3+} \qquad (3)$$
$$Mn^{3+} + OH^- \rightarrow Mn2^+ + OH^\bullet \qquad (4)$$

Therefore, the exchange interaction of Mn^{2+}/Mn^{3+} enhances the lifetime of captured photogenerated carriers (e^- or h^+) in ZnO nanorods. Accordingly, there is more time for photogenerated carriers to contribute to the photocatalytic process before recombination. These results are in good agreement with the results presented by Khani and Martínez-Vargas [44, 45].
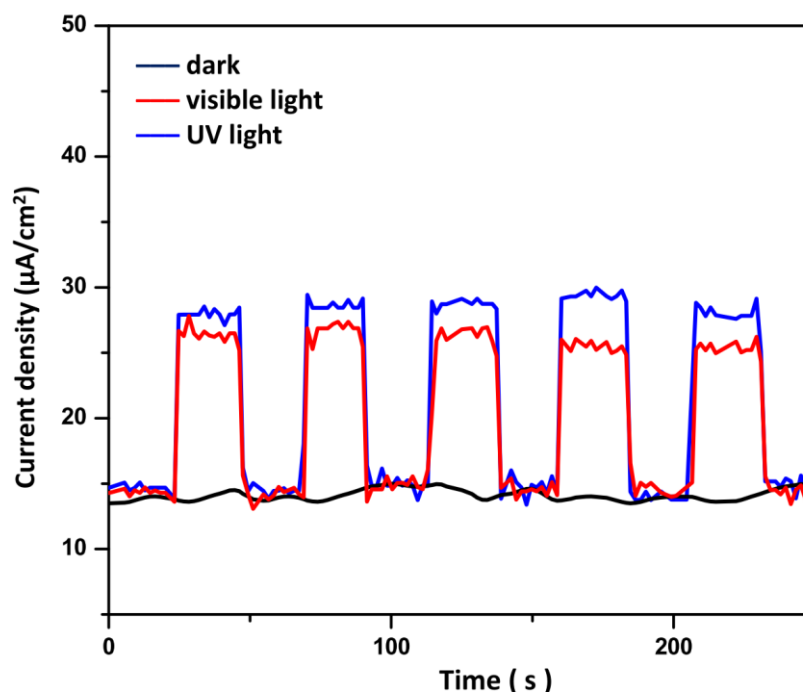

Figure 7. The recorded amperometric response of $Mn_{0.15}Zn_{0.85}O$ nanorods/GCE in 0.1 M PBS pH 4.0 at 0.35 V in injections of 100 µM Gallic acid under darkness and successive periodic turn on and off (visible and UV) light conditions.

In order to examine the photocatalytic degradation performance of the prepared $Mn_{0.15}Zn_{0.85}O$ in UV radiation, the direct ultraviolet radiation (Blank), ZnO and P25 were selected as the control test. It can be seen from Figure 8a that the RhB concentration of the blank group has almost no change under UV light, it proved that RhB is difficult to degradation by UV light alone. After the addition of $Mn_{0.15}Zn_{0.85}O$, ZnO and P25, RhB degradation was more obvious, which confirmed that RhB was removed by catalyst under UV radiation. Obviously, the degradation efficiency of $Mn_{0.15}Zn_{0.85}O$ was significantly higher than degradation efficiencies of ZnO and P25. After 120 minutes of UV radiation, the removal efficiency of RhB reached 84%. The synthesized $Mn_{0.15}Zn_{0.85}O$ was an excellent photocatalyst and had a great application prospect in organic degradation and removal. In Figure 8b, the $-lnC_t/C_0$ corresponding to each photocatalyst was basically linearly related to reaction time t, thus manifesting that RhB degradation followed the quasi-first-order reaction kinetics. The reaction rate constants (k) of blank, P25, ZnO and $Mn_{0.15}Zn_{0.85}O$ are 0, 0.00351, 0.00984 and 0.000.0166 min^{-1}, respectively. $Mn_{0.15}Zn_{0.85}O$ had the strongest UV photocatalytic activity. Compared with ZnO, the photocatalytic degradation performance was significantly improved by the Mn introduction. Mn enhanced the UV light absorption of $Mn_{0.15}Zn_{0.85}O$, and enhanced its UV light utilization. The synthesized $Mn_{0.15}Zn_{0.85}O$ had uniform and regular morphology, and more adsorption active sites were exposed on each crystal surface, which was conducive to the utilization of UV light and the adsorption of RhB. The presence of Mn doped ZnO nanorods leads to the generation of photoexcited electron hole pairs in ZnO nanorods under UV irradiation. It could promote the separation of electrons and holes and slow down their recombination [46]. It greatly improved the photocatalytic performance. In addition, ZnO nanorods mixed by Mn could better provide more catalytic current than un-doped samples under UV illumination. Thus, it greatly increased the free carrier concentration, facilitated the generation of more strong oxidizing holes (h^+) and activated radicals, and finally accelerated RhB degradation and removal [47].
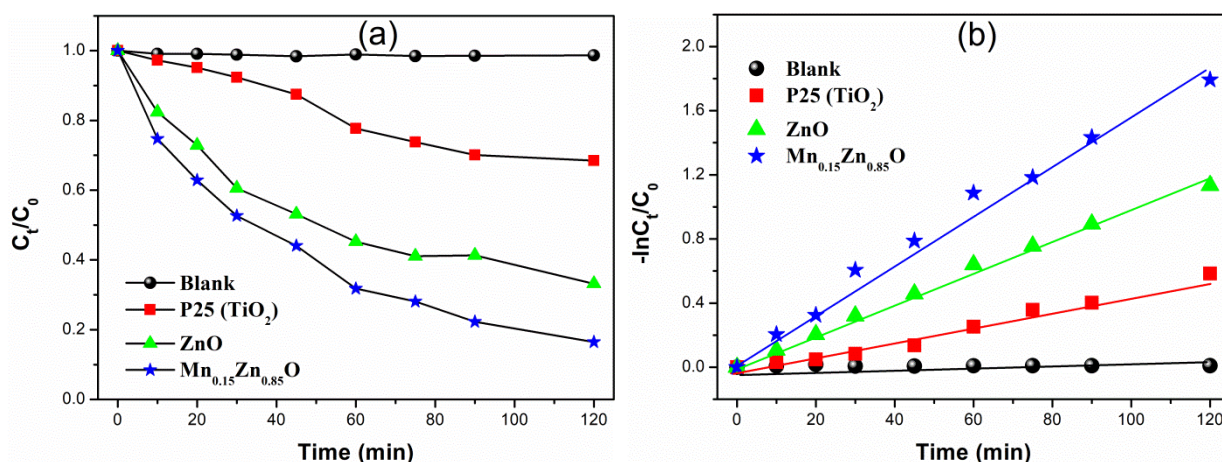

Figure 8. Photodegradation RhB performance (a) and degradation rate (b).

4. CONCLUSION

This study was focused on photocatalytic activity of vertically-aligned $Mn_xZn_{1-x}O$ nanorods by structural, optical and electrochemical analyses. The uniform and dense array $Mn_xZn_{1-x}O$ nanorods

were electrodeposited on ITO coated glass and GCE substrates. The structural studies showed the wurtzite structure for ZnO and Mn_2O_3 impurity phase were observed for synthesized $Mn_xZn_{1-x}O$ samples. Optical study exhibited the edges of absorption spectra were blue-shifted with increasing dopant concentrations which attributed to the variation in the optical band gap value. The photocatalytic performance of $Mn_xZn_{1-x}O$/GCE was studied through electrochemical determination of Gallic acid. Ampermetric analyses showed that the electrocatalytic current density was slightly increased with increasing the dopant concentration in ZnO nanorods. The $Mn_{0.15}Zn_{0.85}O$ nanorods/GCE showed the highest stability response to determine Gallic acid. The photoelectrocatalytic ability of the modified electrode was investigated in dark and under light irradiation conditions. Results showed that the catalytic current responses were increased remarkably under illumination condition and oxidation of Gallic acid was catalyzed by an electron of ZnO conducting bound. Thus, photo-illumination can promote the rate of electron transfer in the electrochemical process. Doping Mn in ZnO lattice exhibits more catalytic current because of increasing the electrical and the free carrier concentration which is donated by zinc interstitials and oxygen vacancy defects. The selectivity and interference response and applicability of the prepared electrode in the real sample were investigated. The RhB photocatalytic degradation performance of $Mn_{0.15}Zn_{0.85}O$ was significantly improved by the Mn introduction, and $Mn_{0.15}Zn_{0.85}O$ showed a favorable performance on RhB degradation and removal.

References

1. J. Rouhi, C.R. Ooi, S. Mahmud and M.R. Mahmood, *Electronic Materials Letters*, 11 (2015) 957.
2. H. Karimi-Maleh, M. Sheikhshoaie, I. Sheikhshoaie, M. Ranjbar, J. Alizadeh, N.W. Maxakato and A. Abbaspourrad, *New Journal of Chemistry*, 43 (2019) 2362.
3. B.O. Chin, Y.N. Law and A.W. Mohammad, *Renewable and Sustainable Energy Reviews,* 81 (2018) 536.
4. A.E.H. Machado, L.M. dos Santos, K.A. Borges, P. Batista, V. Borges de Paiva, P.S. Müller Jr and M. França, *Solar radiation*, 15 (2012) 339.
5. J. Rouhi, S. Mahmud, S.D. Hutagalung, N. Naderi, S. Kakooei and M.J. Abdullah, *Semiconductor Science and Technology*, 27 (2012) 065001.
6. F. Zhang, X. Wang, H. Liu, C. Liu, Y. Wan, Y. Long and Z. Cai, *Applied Sciences*, 9 (2019) 2489.
7. L. Zhang, T. Kanki, N. Sano and A. Toyoda, *Separation and purification technology*, 31 (2003) 105.
8. S.S. Al-Shamali, *Australian Journal of Basic and Applied Sciences*, 7 (2013) 172.
9. S. Fatin, H. Lim, W. Tan and N. Huang, *International Journal of Electrochemical Science*, 7 (2012) 9074.
10. H. Karimi-Maleh and O.A. Arotiba, *Journal of colloid and interface science*, 560 (2020) 208.

11.   C. Dette, M.A. Pérez-Osorio, C.S. Kley, P. Punke, C.E. Patrick, P. Jacobson, F. Giustino, S.J. Jung and K. Kern, *Nano letters*, 14 (2014) 6533.
12.   M. Alimanesh, J. Rouhi and Z. Hassan, *Ceramics International*, 42 (2016) 5136.
13.   S. Al Jitan, G. Palmisano and C. Garlisi, *Catalysts*, 10 (2020) 227.
14.   H. Karimi-Maleh, K. Cellat, K. Arıkan, A. Savk, F. Karimi and F. Şen, *Materials Chemistry and Physics*, 250 (2020) 123042.
15.   J. Rouhi, S. Mahmud, S. Hutagalung and S. Kakooei, *Micro & Nano Letters*, 7 (2012) 325.
16.   R. Hassanzadeh, A. Siabi-Garjan, H. Savaloni and R. Savari, *Materials Research Express*, 6 (2019) 106429.
17.   J. Rouhi, C.R. Ooi, S. Mahmud and M.R. Mahmood, *Materials Letters*, 147 (2015) 34.
18.   M. Negahdary, A. Asadi, S. Mehrtashfar, M. Imandar, H. Akbari-Dastjerdi, F. Salahi, A. Jamaleddini and M. Ajdary, *International Journal of Electrochemical Science*, 7 (2012) 5185.
19.   G. Nagaraju, G.C. Shivaraju, G. Banuprakash and D. Rangappa, *Materials Today: Proceedings*, 4 (2017) 11700.
20.   C. Tian, A. Wu, M. Jiang, Z. Liang, B. Jiang and H. Fu, *Chemical communications*, 48 (2012) 2858.
21.   A. Abdullah, M.Á. Garcia-Pinilla, S.C. Pillai and K. O'Shea, *Molecules*, 24 (2019) 2147.
22.   A. Khodadadi, E. Faghih-Mirzaei, H. Karimi-Maleh, A. Abbaspourrad, S. Agarwal and V.K. Gupta, *Sensors and actuators b: chemical*, 284 (2019) 568.
23.   C.B. Ong, L.Y. Ng and A.W. Mohammad, *Renewable and Sustainable Energy Reviews*, 81 (2018) 536.
24.   H. Karimi-Maleh, C.T. Fakude, N. Mabuba, G.M. Peleyeju and O.A. Arotiba, *Journal of colloid and interface science*, 554 (2019) 603.
25.   F. Chahshouri, H. Savaloni, E. Khani and R. Savari, *Journal of Micromechanics and Microengineering*, 30 (2020) 075001.
26.   H. Savaloni, R. Savari and S. Abbasi, *Current Applied Physics*, 18 (2018) 869.
27.   R. Savari, H. Savaloni, S. Abbasi and F. Placido, *Sensors and Actuators B: Chemical*, 266 (2018) 620.
28.   C. Zou, L. Shao, L. Guo, D. Fu and T. Kang, *Journal of Crystal Growth*, 331 (2011) 44.
29.   H. Savaloni and R. Savari, *Materials Chemistry and Physics*, 214 (2018) 402.
30.   R. Dalvand, S. Mahmud and J. Rouhi, *Materials Letters*, 160 (2015) 444.
31.   K. Tanaka, K. Fukui, S. Murai and K. Fujita, *Applied physics letters*, 89 (2006) 052501.
32.   K.P. Bhatti, S. Chaudhary, D.K. Pandya and S.C. Kashyap, *Solid state communications*, 136 (2005) 384.
33.   J. Zhang, R. Skomski and D.J. Sellmyer, *Journal of Applied Physics*, 97 (2005) 10D303.
34.   J. Rouhi, S. Kakooei, S.M. Sadeghzadeh, O. Rouhi and R. Karimzadeh, *Journal of Solid State Electrochemistry*, 24 (2020) 1599.
35.   Y. Yang, X. Chen, Y. Feng and G. Yang, *Nano letters*, 7 (2007) 3879.
36.   N.S. Sabri, A.K. Yahya and M.K. Talari, *Journal of luminescence*, 132 (2012) 1735.
37.   A.S. Menon, N. Kalarikkal and S. Thomas, *Indian Journal of NanoScience*, 1 (2013) 1.
38.   L. Feng, W. Lu, J. Liu, D. Li, L. Hu and C. Xu, *Electrochimica Acta*, 331 (2020) 29.
39.   N. Naderi, M. Hashim and J. Rouhi, *International Journal of Electrochemical Science*, 7 (2012) 8481.
40.   F. Zhou, W. Jing, P. Liu, D. Han, Z. Jiang and Z. Wei, *Sensors*, 17 (2017) 2214.
41.   L.-l. Wang, W. Ma, J.-l. Ma and G.-q. Shao, *International Journal of Electrochemical Science*, 14 (2019) 9150.
42.   Z. Barzgari, A. Ghazizadeh and S.Z. Askari, *Research on Chemical Intermediates*, 42 (2016) 4303.
43.   R. Marotti, D. Guerra, C. Bello, G. Machado and E. Dalchiele, *Solar Energy Materials and Solar Cells*, 82 (2004) 85.

44.   Z. Khani, D. Schieppati, C.L. Bianchi and D.C. Boffito, *Catalysts*, 9 (2019) 949.
45.   B.L. Martínez-Vargas, M. Cruz-Ramírez, J.A. Díaz-Real, J. Rodríguez-López, F.J. Bacame-Valenzuela, R. Ortega-Borges, Y. Reyes-Vidal and L. Ortiz-Frade, *Journal of Photochemistry and Photobiology A: Chemistry*, 369 (2019) 85.
46.   Z. Jiang, L. Feng, J. Zhu, X. Li, Y. Chen and S. Khan, *Ceramics International*, 46 (2020) 98.
47.   X. Li, B. Yang, C. Xu, J. Liu, W. Lu, S. Khan and L. Feng, *Journal of Materials Science: Materials in Electronics*, 30 (2019) 57.